Microporous and Mesoporous Materials 376 (2024) 113196

Contents lists available at ScienceDirect

Microporous and Mesoporous Materials

journal homepage: www.elsevier.com/locate/micromeso

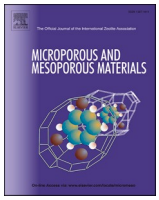

A Mayan-inspired DAPI fluorophore stabilized and enhanced through sorption on palygorskite

Roberto Giustetto [a,b,c,e,*], Gabriele Ricchiardi [b,d,e], Francesca Bonino [b,d,e], Nadia Barbero [b,d,e,f]

[a] Department of Earth Sciences, University of Turin, via Valperga Caluso 35, 10125, Torino, Italy
[b] NIS (Nanomaterials for Industry and Sustainability) Centre, via Quarello 15/A, 10135, Torino, Italy
[c] INFN (National Institute of Nuclear Physics), via P. Giuria 5, 10125, Torino, Italy
[d] Department of Chemistry, University of Turin, via P. Giuria 7, 10125, Torino, Italy
[e] INSTM (National Inter-University Consortium for Materials Science and Technology), via P. Giuria 7, 10125, Torino, Italy
[f] ISSMC-CNR (Istituto di Scienza, Tecnologia e Sostenibilità per lo Sviluppo dei Materiali Ceramici), via Granarolo 64, 48018, Faenza, Italy

ARTICLE INFO

Keywords:
Palygorskite
DAPI
Hybrid nanocomposite
Host/guest interactions

ABSTRACT

DAPI (4′,6-diamidino-2-phenylindole, di-hydrochloride) is a photoactive dye used as a fluorescent marker for nucleic acids, due to its high affinity for the major groove in the DNA double helix. By following a *Mayan-inspired* recipe (namely grinding, heating and washing in H_2O), the DAPI molecule was fastened to the microporous framework of palygorskite – a clay mineral used to produce the famed *Maya Blue* pigment, whose fibrous crystals are carved by surface grooves similar in size to those of DNA – in order to obtain a newly designed fluorescent material. This hybrid composite was investigated with a multi-analytical approach, which includes FE-SEM-EDS, BET-specific surface area (SSA)/micropore volume measurements, thermogravimetry, UV–vis, fluorescence and FT-IR spectroscopies. Supramolecular interactions form between the clay and the dye *already* after grinding, apparently involving a two-step binding process. Evidence is found of an incipient, electrostatic interaction between cationic DAPI and the negatively charged surface of the palygorskite fibrils, which then evolves in H-bonding interaction between the dye amine groups and the zeolitic and/or structural water in the clay surface grooves. Heating and washing in H_2O seemingly deteriorate the composite morphology and stability, jeopardizing – rather than strengthening – the previously formed host/guest interactions. This hybrid composite, with remarkable stability and appreciable quantum yield, is potentially fit to be used as a low-cost, fluorescent material for applications such as spectrum manipulation technologies, sensors, optical devices, imaging and design-targeted drug-delivery systems.

1. Introduction

Stabilized organic molecules with functional features can substitute metals or semiconductors in various technological applications (e.g., in dye sensitized solar cells, tailoring of material properties, optoelectronics and optical non-linear – ONL, properties, etc.), depending on their structural arrangement and vibrational freedom [1,2], which in turn rule their electronic coupling affecting optical and charge-transfer properties [3–5]. Their stabilization on a substrate can be modulated by various supramolecular approaches – e.g., metal-organic frameworks (MOF), synthesis of crystals and thin films, epitaxial growth or sorption on a host matrix [6–9]. The enhancement in the stability of the dye embedded in a nanostructure allows broadening the conditions in which this species can operate and its use for a given purpose, like for example photoactivity or sensitivity to pH [10].

For what concerns hybrid composites, *Maya Blue* – a stable pigment used by ancient Mayas in Mexico (mostly Yucatàn peninsula), whose colour and structure can resist to harsh acids or alkali attacks – holds a prominent place. Formed by the indissoluble coupling of the palygorskite clay mineral [ideal formula: $(Mg,Al)_4Si_8O_{20}(OH)_2(OH_2)_4 \bullet 4H_2O$; PALY hereafter) with the frail indigo dye, *Maya Blue* is an ancestor of modern host/guest composite materials [11]. PALY, an end-member in a polysomatic series with sepiolite [12], is a mixture of a monoclinic (Space Group: *C2/m*) and an orthorhombic polymorph (Pbmn) [13,14]. Its fibrous crystals (‘fibrils’ or ‘laths’; Fig. 1a) [15] are elongated along [001] with length usually ≤ 5 μm. Its structure shows a continuous, waving tetrahedral (T) sheet, due to a periodical inversion in the apical oxygens orientation, and an octahedral (O) one broken in

* Corresponding author. Department of Earth Sciences, University of Turin, via Valperga Caluso 35, 10125, Torino, Italy.
E-mail address: roberto.giustetto@unito.it (R. Giustetto).

https://doi.org/10.1016/j.micromeso.2024.113196
Received 10 November 2023; Received in revised form 13 May 2024; Accepted 23 May 2024
Available online 24 May 2024

'ribbons' that run along the *z* axis [16]. This structure is crossed by tunnels (maximum effective width: 0.64 × 0.37 nm), *z*-axis elongated and filled by weakly bound zeolitic H_2O and tightly bound structural OH_2. The latter completes the coordination of the Mg ions at the borders of the O ribbons (Fig. 1c). More loosely bound physisorbed H_2O covers the external surface of the laths. Both physisorbed and zeolitic H_2O are lost by heating (80–100 and 120–190 °C, respectively), but higher temperatures are needed to trigger loss of structural OH_2 (>250 °C) [17,18]. The surface of the PALY laths is carved by grooves, resulting from the half-open structural tunnels exposed on the {100}, {110} and {010} crystal faces (Fig. 1b) [19].

PALY can stabilize the guest indigo molecule inside the inner tunnels permeating its structure and in the grooves that carve the laths surface, thus justifying the steadiness of *Maya Blue* [20–24]. These findings opened a fruitful field of research aimed at replicating the *Maya Blue* features using other molecules as guests – obtaining hybrid materials with physicochemical properties useable in Materials Science or Cultural Heritage [25]. Stable composites with 4-Cl-thioindigo and quinalizarin were produced [26], as well as with thioindigo [27,28], 'Ciba Brilliant Pink' and isatin, which are absorbed in the PALY tunnels [29,30]. Red-to-purplish adducts were obtained with methyl red and alizarin [31–35]: the former is stuck in the PALY tunnels (its colour being unvaried after acid/alkali attacks), the latter binds to the fibre surface (its colour changing with pH fluctuations). The affinity of PALY for absorbing dyes also paved the way for other applications – i.e., pollutants removal from wastewaters [36,37]. Mu and Wang [38] issued a detailed review on the potentiality of PALY as a dye adsorbent.

Organic fluorophores play a leading role in many fields of application – such as biological imaging, spectral correction of light sources, sensing and diagnostics [39–41]. As such, their sorption on microporous clays offers interesting perspectives. A hybrid pigment was obtained by associating a coumarin-derivative dye (FY-10G) to PALY, enhancing fluorescence, thermal and photo-stability with respect to the dye alone [42]. Sepiolite (similar to PALY, but with larger tunnels) was used for sorption of methylene blue, methyl red, anthocyanin- and pyranoanthocyanin-analogues, providing enhanced resistance with respect to thermal, redox and biological degradation [43,44]. Stabilization of these *Mayan-inspired* composites occurs by hooking the organic species to the host clay, achieved through shape recognition and formation of H-bonds and/or electrostatic interactions.

In organic materials, interactions by surface grooves have important implications – e.g., in prebiotic chemistry (e.g., catalysis and protection of amino acids) [45–47]. A paradigmatic application is represented by the use of DAPI for DNA detection. DAPI (4′,6-diamidino-2-phenylindole, di-hydrochloride) is a blue, non-toxic, fluorescent stain capable of binding to DNA enhancing its fluorescence and providing an imaging of the genetic material in cells [48]. It is also used as an anti-parasitic, -biotic, -viral and -tumor agent [49]. Its molecule has a joint phenyl and indole chromophore, each with an auxochromic amidino group, and exhibits a wide array of interactions binding both in the minor [50,51] and major DNA groove [52], by intercalation and other interactions [53–58]. In cationic form, its molecule binds to adenine-thymine (AT) clusters in the DNA minor groove with a reversible interaction (Fig. 1d) [59,60]. Binding produces a ≈ 20-fold fluorescence increase ("Light-Switch" effect) [61] proportional to the DNA amount, with an emission maximum at ≈ 460 nm [62]. DAPI also binds to RNA, but the fluorescence is diminished and shifted at ≈ 500 nm [63,64].

Since the major groove of DNA and the grooves on the surface of the PALY laths bear some resemblances – both in terms of geometry and chemical environment, we explore the possibility for DAPI to interact with PALY forming a stable composite ('***PALY@DAPI***' hereafter) with enhanced fluorescence. Complexation of PALY with DAPI has both a fundamental and practical interest, as stabilizing the labile dye moiety in a solid matrix may lead to a robust, metal-free, fluorophore for optical, imaging and drug-delivery applications.

2. Materials and methods

2.1. Materials

A natural PALY specimen from Mexico (State of Chiapas) was used. PALY was preferred to sepiolite since the latter – though disposing of larger tunnels (maximum effective width: 1.06 nm) [65] – has a weaker structure [66]. Purification of PALY [17,67], aimed at eliminating impurities and promoting dispersion/disaggregation of the bundles (to favour guest complexation) [68], consisted of: i) hand-grinding in agate mortar and removal of macroscopic impurities; ii) suspension in deionized H_2O, isolating the floating fraction from residual impurities (e.g., calcite and quartz) and the more entangled bundles, which settle at the bottom; iii) soaking in diluted HCl (approx. 2.4 M, 20 % v/v of concentrated 37 % w/w solution) to eliminate fine-grained carbonates, followed by washings in deionized H_2O and filtering. After purification, X-ray powder diffraction (XRPD) proved PALY to be the only detectable phase (Supporting Information, Fig. S1).

The DAPI specimen used in this study, in the form of a yellow powder, was purchased from Sigma-Aldrich (Line # 000040, Cod. No. D9542-50 MG) and used without purification.

2.2. Synthesis of the 'PALY@DAPI' adduct

The hybrid composite synthesis was modeled upon the laboratory

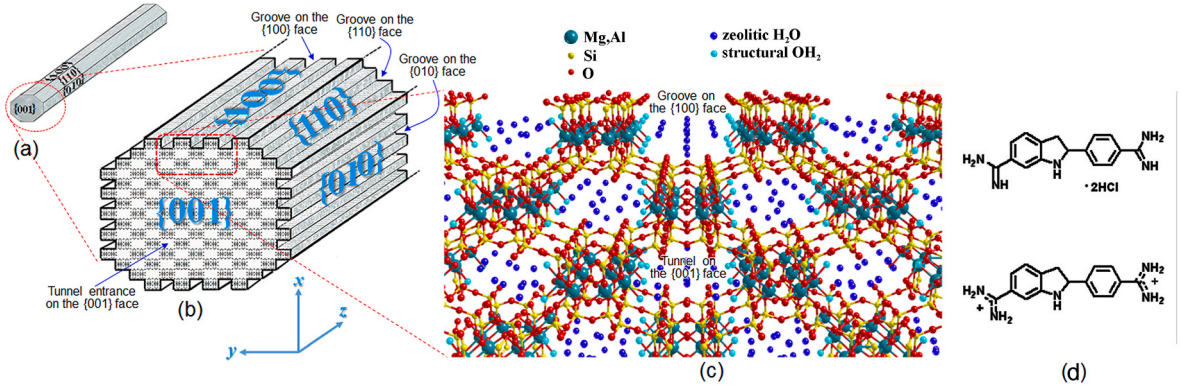

Fig. 1. a) detail of a palygorskite fibril (lath) with indexing of the crystal faces; b) magnification of the fibril tip, with indication of the surface grooves and inner tunnels (mutual dimensions of the fibril and crystal structure not in scale); c) the crystal structure of palygorskite, observed along [001], complete with zeolitic H_2O and structural OH_2 (H atoms not shown for sake of simplicity); d) the molecule of 4′,6-diamidino-2-phenylindole, di-hydrochloride (DAPI) in neutral (up) and cationic (down) form.

preparation of *Maya Blue* from pure precursors [27,69–71]: i) the purified PALY powders were mixed and ground in an agate mortar with DAPI 2 wt % (maximum indigo amount absorbable on PALY [66]; **PALY + DAPI MM**, hereafter); ii) the mixture was soaked in H_2O in a Petri dish and heated from room *T* until 160 °C for 24 h, with a 20 °C/h ramp (**PALY + DAPI H**, hereafter). Maximum temperature was chosen in order to favour activation of the clay and not exceed the dye sublimation point; iii) after heating, the powders were washed for 24 h under H_2O flux to remove any unbound DAPI cluster (**PALY + DAPI W** hereafter).

The '*PALY@DAPI*' adduct has a light yellowish hue after grinding, reminiscent of the deep yellow colour of the dye. This hue is maintained with no appreciable fading after heating, but washing in H_2O is responsible for a slight bleaching (Supporting Information, Fig. S2).

2.3. Methods

Field Emission Scanning Electron Microscopy (FE-SEM) data were collected with a Tescan S9000G FESEM 3010 microscope (30 KeV) equipped with a high-brightness Schottky emitter. The powder samples were deposited on a stub coated with a conducting adhesive and with a 5 nm Cr sputtered film. Elemental EDS analyses and maps were obtained with an Oxford Instruments Ultim Max SDD analyzer in the SEM column.

Adsorption/desorption measurements with N_2 at 77 K were performed using a Micromeritics 3Flex sorption analyzer. Before analysis, samples (ca. 100 mg) were treated overnight in high vacuum at 100 °C (heating ramp: 2 °C/min). Specific surface areas (SSAs) were evaluated by employing the Brunauer-Emmett-Teller (BET) equation in the $0.02 < p/p^0 < 0.2$ range. The micropore volume was extrapolated from the t-plot curve derived from the adsorption branch of N_2 isotherms at 77 K, considering the statistical thickness range 4 Å < t < 6.5 Å.

UV–visible (UV–Vis) data in transmittance mode were collected in the 800-200 nm range on DAPI in aqueous solution by varying pH, using a Varian Cary 300 Bio spectrophotometer. UV–visible–NIR data in diffuse reflectance (DR) mode were collected in the 2500-200 nm range on both precursors (diluted in Teflon, for DAPI) and on the '*PALY@DAPI*' adduct in all synthesis steps, using a Varian Cary 5000 spectrophotometer.

Infrared (IR) absorption data were collected in air at room *T* on a FT-IR Bruker Vector 70 spectrometer with a 2 cm^{-1} resolution (64 scans for each spectrum) – in ATR mode with a diamond prism on both precursors and in transmission mode on pellets of '*PALY@DAPI*' in all synthesis steps.

XRPD data were collected on an automated Miniflex 600 Rigaku diffractometer in Bragg-Brentano geometry in θ-θ setup, Cu-Kα radiation and a zero-background flat sample holder.

Fluorescence emission spectra were collected on a Horiba Jobin Yvon Fluorolog 3 TCSPC fluorimeter, equipped with a 450-W Xenon lamp. A Hamamatsu R928 photomultiplier was used to acquire fluorescence spectra in steady state mode. Absolute quantum yield was measured with an integrating sphere combining Quanta-φ with Fluorolog 3, the reported values being averaged on 3 measurements. Solid samples were excited at 370 nm and fluorescence signal recorded from 400 to 700 nm. DAPI was diluted in SiO_2 (previously calcined at 800 °C for 1 h) to obtain a Kubelka-Munk (KM) value of 0.1 (spectrum not reported for sake of brevity). PALY and '*PALY@DAPI*' adducts in all synthesis steps were measured as prepared, with no dilution. Lifetimes were measured by the time correlated single photon counting method (Horiba Jobin Yvon), using a 455 nm Horiba Jobin Yvon NanoLED as excitation source and an impulse repetition frequency of 1 MHz positioned at 90° with respect to a TBX-04 detector, and calculated using the DAS6 decay analysis software.

TGA experiments were performed by using a TGA Q600 SDT instrument on ≈ 10 mg specimens, in both N_2 (100 ml min^{-1} nitrogen flow) and dried air. Weight loss (%) vs. temperature was evaluated in the 30–800 °C range, with a 10 °C/min heating ramp.

Density functional theory (DFT) calculations were performed on the DAPI molecule with the aim of assigning each IR-maximum to the proper vibrational mode. In order to mimic the surroundings of the dye may in the adopted experimental setups, two models were considered: (i) an isolated DAPI molecule and (ii) a DAPI molecule hydrated by five H_2O molecules forming H-bonds with polar groups. Both models were optimized at the B3LYP/cc-pVDZ using the Gaussian16 software [72]; frequencies were calculated at the same level of theory. Structures of the optimized models appear in the Supporting Information, Fig. S3 and Table S1.

3. Results

3.1. FE-SEM-EDS analyses

In raw unpurified PALY (Fig. 2a), fibrils are scattered and dense bundles are rare; the thinner laths have an average ≈ 4 ± 1 μm length and 26 ± 6 nm width. Impurities, mostly carbonates, are also present (Supporting Information, Figs. S4 and S5). After purification (see Section 2.1), the PALY laths become shorter (<1 ± 0.5 μm) and more aggregated, with crenulated surfaces at higher magnifications (Fig. 2 b and Supporting Information, Figs. S6 and S7). Their chemical formula (obtained by electron probe microanalyses collected on a pressed pellet and computed on 26 oxygens; total water content extrapolated by TGA [73]) is: $(Mg_{2.25}, Al_{1.63}, Fe_{0.25}, K_{0.06}, Na_{0.01})(Si_{7.95},Al_{0.05})[O_{19.95}(OH)_{2.03}(OH_2)_{4.05}] \bullet 4.78H_2O]$ [17]. Solid DAPI appears in the form of bulky prismatic crystals, even > 10 μm long (Fig. 2c); EDS elemental maps show significant presence of N and Cl, confirming the hydrochloride nature of the molecules (Supporting Information, Fig. S8).

As far as the composite is concerned, in **PALY + DAPI MM** (Fig. 2d) the host fibres seem less dense, probably because grinding favour cleavage and scattering in the PALY laths orientation. However, the thickness of the thinner fibrous units grows up to ≈ 38 ± 7 nm, suggesting that crushing and complexation with DAPI may favour the pairing of doublets or triplets of PALY laths, stuck with one another and with parallel orientation. Even at higher magnifications, DAPI clusters are not observed – with EDS detecting a very low and homogeneously distributed Cl amount (≈ 0.1 wt %, a marker for DAPI; Supporting Information, Figs. S9 and S10). These evidences suggest that grinding causes the DAPI crystals to dissolve completely on the hydrated surface of the host matrix. In **PALY + DAPI H**, the doublets/triplets of laths – their thickness unvaried (34 ± 5 nm) – tend to further aggregate with one another, maintaining mostly parallel courses and forming thicker bundles (even > 500 nm: Fig. 2e). This behavior is consistent with the migration of water soluble components to the surface of the fibrils due to heating and consequent dehydration (so-called "caking" effect), followed by formation of solid inter-particle "bridges" as loss of water proceeds [74,75]. Still, no clear evidence of DAPI is detected by EDS (Cl ≈ 0.2 wt %). After washing in H_2O (**PALY + DAPI W**), the composite aspect reveals that some damage has occurred. The host fibrous units (pairs/triplets of laths, thickness ≈ 39 ± 6 nm) become shorter (even < 500 nm) and with rounded tips, being packed in messy aggregates in which the fibrous habitus is less evident (Fig. 2f). This is consistent with the morphological decay shown by the PALY fibrils after loss of water due to thermal treatment, typical also of *Maya Blue* [76]. Cl is not even measured by EDS, implying that the dye amount is well below the detection threshold.

All these evidences suggest that crushing promotes a gradual aggregation of the PALY fibrils, favouring formation of couples and triplets of laths in which DAPI is efficiently spread on the surfaces exposed outwards (and possibly also on those leaning against each other), probably interacting with the host water. This process intensifies after heating, where thick bundles of fibrous units are observed. Final washing reveals that a certain decay occurs, as most fibres are broken, randomly oriented and with smoothened edges. These treatments are thus likely to weaken – rather than enhance – the composite stability.

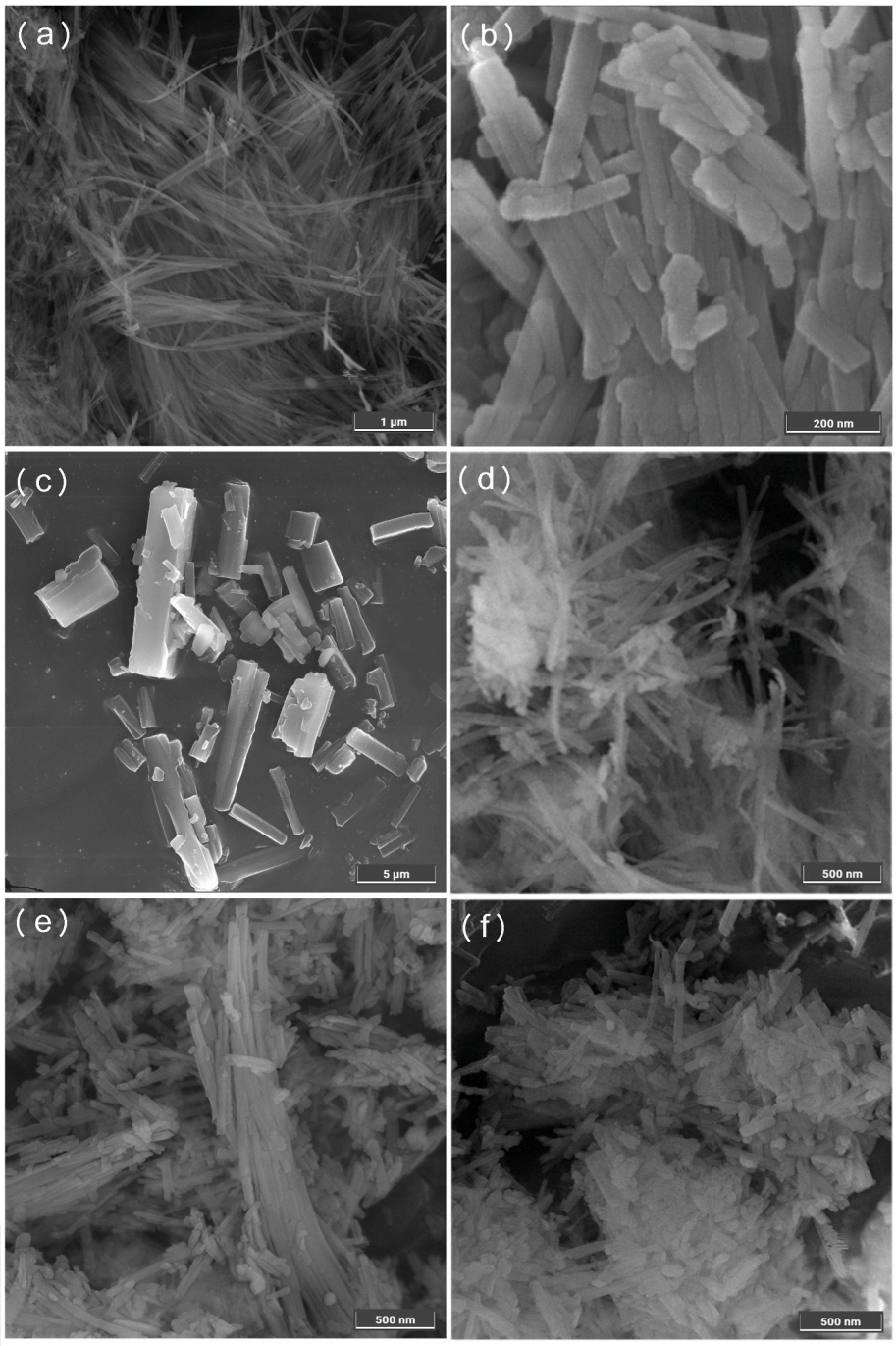

Fig. 2. High-resolution FE-SEM images of: a) raw palygorskite fibrils (or laths: length ≈ 4 ± 1 µm; width ≈ 26 ± 6 nm); b) palygorskite fibrils after purification (length ≈ < 1 ± 0.5 µm; width ≈ 25.7 ± 7 nm); c) DAPI in powder. High-resolution FE-SEM images of the '*PALY@DAPI*' composite after: d) mixing and grinding (**PALY + DAPI MM**), in which laths are grouped in couples and/or triplets (length ≈ < 1 ± 0.5 µm; width ≈ 38 ± 7 nm); e) heating (**PALY + DAPI H**), in which couples/triplets of laths (length ≈ < 1 ± 0.5 µm; width ≈ 34 ± 5 nm) gather in thicker bundles even 500 nm thick; f) washing in H_2O (**PALY + DAPI W**), in which couples/triplets of laths become shorter (length ≈ < 500 ± 200 nm; width ≈ 39 ± 6 nm) with smoothened edges, forming messy aggregates.

3.2. BET-SSA and micropore volume measurements

Adsorption/desorption isotherms of N_2 for PALY and '*PALY@DAPI*' in all synthesis steps are shown in Fig. 3. Purified PALY has a BET-SSA of 129.0 ± 0.5 m^2/g, which is in agreement with literature data collected in similar experimental conditions [77]. As expected from the related isotherm (reminiscent of type II), the related micropore volume obtained by t-plot is negligible (0.015 cm^3/g; Supporting Information, Table S2).

When PALY is ground with DAPI (**PALY + DAPI MM**), a significant reduction in the BET-SSA occurs (Fig. 3), reaching 75.9 ± 0.3 m^2/g. This decrease, related to the exposed external surface of the fibrous crystals, is consistent with the tendency of the PALY laths to stick to one another forming parallel oriented couples and/or triplets after crushing with DAPI – whose molecules are presumably spread on the crystal faces (as inferred by FE-SEM: see Section 3.1; Fig. 2d). Once heating is applied

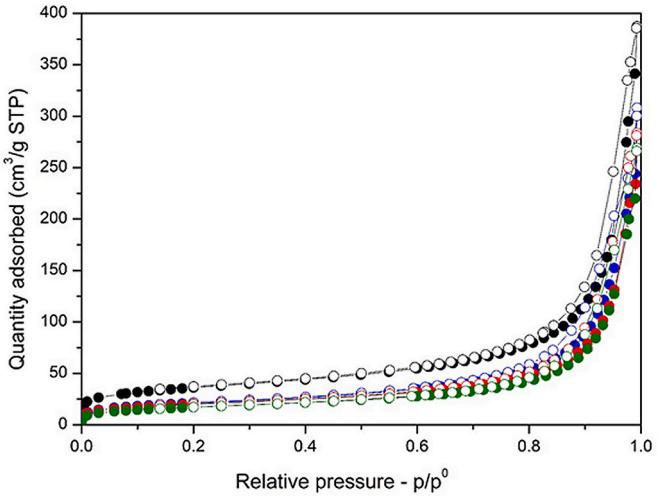

Fig. 3. Volumetric adsorption (full symbols) and desorption (empty ones) isotherms of N_2 at 77 K of PALY (in black), **PALY +_DAPI_MM** (blue), **PALY_+ DAPI_H** (green) and **PALY +_DAPI_W** (red).

(**PALY + DAPI H**), a further moderate decrease in the inter-fibrils porosity is observed – the BET-SSA dropping to 61.8 ± 0.1 m^2/g. Again, this decrease is consistent with the amassment of the above mentioned couples/triplets of laths to form more massive bundles (>500 nm thick), as observed by FE-SEM (see Fig. 2e). After washing in H_2O (**PALY + DAPI W**) this trend reverses, as a modest enhancement in the surface area porosity occurs anew (BET-SSA reaching 71.7 ± 0.2 m^2/g; Supporting information, Table S2). This behavior is consistent with the observed morphological deterioration affecting the composite aspect, in which shorter fibers with smoothened edges tend to group in messy aggregates (see Fig. 2f).

For what concerns the micropore volume, the values of the '*PALY@DAPI*' adduct – though maintaining a similar trend – remain low in all synthesis steps (≤ 0.005 cm^3/g; Supporting information, Table S2). These data confirm that microporosity – at least in the adopted experimental conditions – is hardly accessible and not significant. Though the adoption of higher outgassing temperatures would have rendered the microporosity of the material accessible [77], we chose to maintain experimental conditions more akin to those applied during the composite synthesis (see Section 2.3) rather than overshooting them. Highly vacuum-dehydrated PALY, in fact, has completely different sorption properties that are not relevant to the present study, in which all samples are prepared and handled at ambient conditions in air.

3.3. Absorption and DR UV–Vis spectroscopy

The UV–Vis absorption spectrum of DAPI (5.5 μM) in aqueous solution at pH = 7 appears in Fig. 4 a. No notable change occurs by slightly varying pH; DAPI is insensitive in the 5–10 pH range, its fluorescence remaining unchanged over a 4–11 pH range [62]. Also, no acid/alkali agent liable of trespassing these values was used in the composite preparation.

Solute-solvent H-bonded interactions occur, which involve the hydration shell of the dye molecule [78]. Three main bands appear at ≈ 224, 261 and 344 nm. The last, most intense one is responsible for the yellow hue of the dye [79]; it is not observed for an isolated phenyl or indole chromophore, but it appears in 2-phenyl substituted five-membered N-heterocyclic compounds, probably due to conjugation of both chromophores [80,81]. When brominated on the indole 3rd carbon (Br-DAPI), this band undergoes a ≈ −20 nm blue shift [82]. Its formation is due to two partially overlapping transitions, with different moment polarization [83,84] and involving both chromophores – their moments being polarized on a vector connecting them, consistently with the elongated molecule shape. Two transitions justify the band at 224 nm and one that at 261 nm. Another weak transition is responsible for the shoulder at ≈ 290 nm, which breaks the symmetry of the main band [81].

The DR-UV-Vis spectra of the '*PALY@DAPI*' composite in all synthesis steps appear in Fig. 4 b, together with those of the precursors in powder. PALY has no visible signal, but a unique UV band at ≈ 248 nm. Powdered DAPI shows a sole broad visible band at ≈ 430 nm (and two weak shoulders at ≈ 268 and 314 nm). Its marked asymmetry confirms its correlation with the main band in aqueous solution [81,83,84]. Absorptions in the UV region are not detected in DR mode, due to photoluminescence of the dye. In **PALY + DAPI MM**, the main dye band undergoes a marked blue-shift with respect to pure DAPI, reaching ≈ 364 nm – a position still far from that in aqueous solution (344 nm). Also, two additional UV features appear at ≈ 208 and 268 nm (shoulder), different than those in aqueous solution but reminiscent (at least the latter) of a signal of solid DAPI. These variations confirm the intervened dissolution of the DAPI crystals and solvation on the PALY framework (which contains a relevant amount of H_2O). If compared to that in solution, the magnitude of the main band bathochromic shift (≈ +20 nm) implies that the dye may interact, at some level, with the PALY framework with consequences on its electronic structure. The nature of these interactions – at this stage – is yet unclear, but their strength is not negligible. For example, when DAPI binds to the AT base pairs in the minor-groove of calf thymus DNA [83,85,86], this band undergoes a +10 nm red-shift if compared to that in aqueous solution [79]. Similar, or even higher, red-shifts are also observed when DAPI binds to other molecular matrices [49,78,87], although some DAPI-composites show no appreciable red-shift [88] and, seldom, modest hypsochromic ones are also observed [89]. Yet, when the shift is bathochromic (as in **PALY + DAPI MM**) formation of host/guest interactions is plausible. Besides, the fact that this shift is almost doubled if compared to other solvating matrices (even by considering the different environments) reinforces the

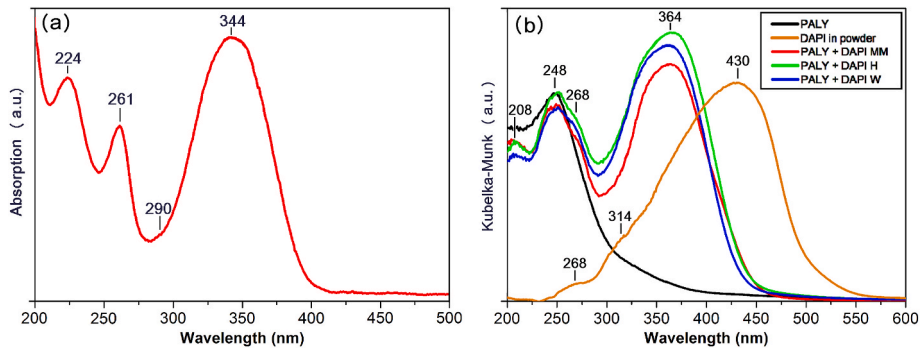

Fig. 4. a) The UV–Vis absorption spectrum of DAPI in aqueous solution; b) The Diffuse Reflectance UV–Vis spectra of PALY (in black), solid DAPI (diluted in Teflon; orange) and the '*PALY@DAPI*' composite in all synthesis steps: **PALY + DAPI MM** (red), **PALY + DAPI H** (green); **PALY + DAPI W** (blue).

assumption that a strong interaction may exist between the clay and the dye (e.g., to obtain an equal red-shift with sodium dodecyl sulfate (SDS) micelles, a 10^3-fold matrix excess with respect to DAPI must be used [49]).

Heating at 160 °C and washing in H_2O do *not* affect the spectral features of the '*PALY@DAPI*' adduct. Such an invariance suggests that these treatments may not alter the nature or strength of the host/guest interactions formed after grinding.

3.4. Fluorescence spectroscopy

Fluorescence data were collected on the '*PALY@DAPI*' adduct in all synthesis steps and on pure PALY and DAPI (in powder and H_2O solution) for comparison purposes (Fig. 5).

PALY has no fluorescence, but DAPI in aqueous solution has an emission peak at ≈ 480 nm [78,79,88,90], which largely shifts to 560 nm in the solid powder. The **PALY + DAPI MM** spectrum maintains the band at ≈ 480 nm (the same of DAPI in aqueous solution) sided by a marked shoulder at ≈ 560 nm. This marked asymmetry suggests that two distinct signals may contribute to the profile – one (more intense) accounting for complexation of DAPI with PALY, the other (shoulder at higher wavelength, i.e., closer to the band of the solid) related to dye clusters on the surface of the PALY fibres. The quantum yield (the number of emitted photons relative to the number of absorbed photons; QY) has a ten-fold increase if compared to that of pure DAPI in aqueous solution (0.42 vs. 0.04). A moderate fluorescence enhancement thus occurs after complexation of the dye with PALY. After heating, the main band of **PALY + DAPI H** undergoes a modest blue-shift at 476 nm, further enhanced (reaching 473 nm) in **PALY + DAPI W**. As expected, the shoulder at ≈ 560 nm progressively decreases, implying that washing favours removal of the superficial dye clusters – leaving only the stabilized DAPI molecules to bind to the PALY framework. This blue-shift could be justified by the bound DAPI molecules gradually sensing the hydration water of PALY at a higher degree as synthesis proceeds, thus enhancing solvation of the complexed dye. This is also confirmed by the QY values, which decrease (becoming more akin to that of DAPI solvated in water) after heating and washing (Table 1). These outcomes not only confirm that interactions between PALY and DAPI form *already* after grinding (consistently with UV–Vis results), but also that the '*PALY@DAPI*' adduct undergoes a certain deterioration after heating and washing in H_2O.

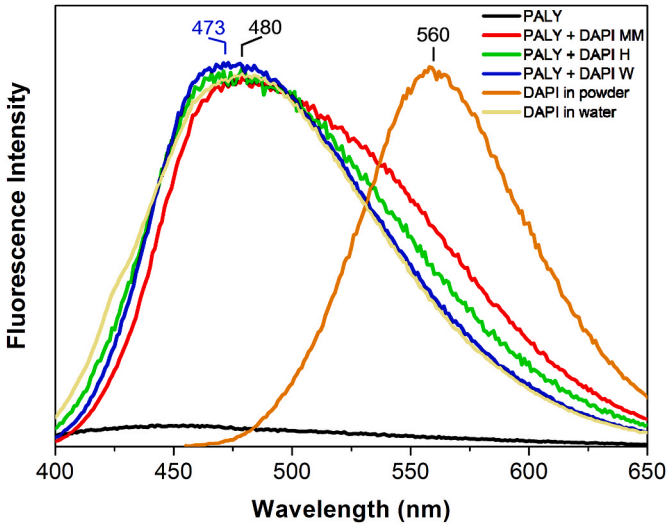

Fig. 5. The fluorescence spectra of PALY (in black), DAPI in aqueous solution (yellow) and solid (orange) and the '*PALY@DAPI*' composite in all synthesis steps: **PALY + DAPI MM** (red), **PALY + DAPI H** (green), **PALY + DAPI W** (blue).

Table 1
Fluorescence emission and QY of DAPI and the '*PALY@DAPI*' adduct in all synthesis steps.

Sample	λem (nm)	φ
DAPI in water [92]	480	0.04
PALY + DAPI MM	480	0.42 ± 0.01
PALY + DAPI H	476	0.15 ± 0.01
PALY + DAPI W	473	0.20 ± 0.03
Solid DAPI	560	0.35 ± 0.02

Time resolved fluorescence analyses of DAPI in aqueous solution and the '*PALY@DAPI*' adducts were also performed, but the interpretation of lifetimes (Supporting Information, Table S3, Fig. S11) is not straightforward. As reported in the literature [85,91], DAPI in H_2O shows two decay times, with a strong dependence from pH. After sorption on PALY, two more decay times appear – whose assignment is troublesome and beyond the scope of this work.

3.5. ATR-FTIR and transmission FTIR spectroscopy

ATR-FTIR spectra were collected on PALY and assignments of the related bands are reported in the Supporting Information, Table S4 (references indicated therein). In the stretching region (3750-2750 cm^{-1}), the signals of all kinds of water (physisorbed, zeolitic H_2O and structural OH_2) and hydroxyls appear. In the bending region (1250-1750 cm^{-1}), a sole mode related to all kinds of water exists at ≈ 1650 cm^{-1}, whose position and intensity reflect experimental conditions (e.g., water loss during calcination, interactions with guests, etc.). Below 1200 cm^{-1}, lattice modes appear (e.g., Si-O-Si and Si-O asymmetric or symmetric stretch). When heated below 300 °C and then re-hydrated, the PALY spectrum undergoes reversible variations, having no effect on the crystal structure [20,32,37]. To the best of our knowledge, the IR spectrum of DAPI has never been published so far. Its pattern was thus calculated with *ab initio* DFT methods, for both an isolated dye molecule and one hydrated by 5 explicitly modeled H_2O molecules. Assignments are reported in Table 2 (first three columns). ATR-FTIR data were then collected on solid DAPI and on a drop of saturated solution of DAPI in H_2O, also containing some undissolved dye. This expedient was aimed at overcoming the difficulty of collecting IR spectra in water solution, taking advantage of the fact that the ATR-IR spectrum of H_2O – compared to that in transmission – has weak signals. As such, it was used as a reference to measure the solution/suspension. The two spectra (Supporting Information, Fig. S12) are quite similar, possibly due to coexistence of solute and solid DAPI in the water drop. However, the bands related to H-bond-forming groups show some shifts in water, consistent with those calculated for the hydrated models. The observed maxima positions are reported in Table 2 (columns 4 and 5), referring to their specific assignments. In some cases, these assignments must be considered approximate, due to the strong coupling among modes.

Transmission IR spectra were collected on the '*PALY@DAPI*' composite in all synthesis steps. The adoption of a different setup – transmission rather than ATR – is justified by the fact that the latter setting does not allow, due to its lower sensitivity, an apt identification of the weak DAPI signals when adsorbed on PALY. These spectra, compared to those of pure PALY and solid DAPI, appear in Fig. 6 a; a magnification in the 1650-1200 cm^{-1} range appears in Fig. 6 b.

The dye modes positioned in the 3800-2800 and 1700-1600 intervals and below 1250 cm^{-1} are hidden under the stretching/bending maxima of the different kinds of water/hydroxyls and lattice vibrations of PALY. However, as no remarkable PALY signal occurs in the 1600-1250 cm^{-1} range, most of the DAPI 'fingerprint' can be appreciated there (Fig. 6b). Its variations and those related to the clay framework are commented hereafter.

In **PALY + DAPI MM**, several modes between 1570 and 1280 cm^{-1} are similar to those of the pure dye (e.g., at 1544, 1481 and 1461 cm^{-1}).

Table 2
Calculated FT-IR active signals for DAPI (4′,6-diamidino-2-phenylindole, di-hydrochloride) – both isolated and hydrated by 5 H_2O molecules – compared with experimental data collected on DAPI in aqueous suspension and powder. The DAPI vibrational modes appearing in the spectra of the '*PALY@DAPI*' composite (Fig. 6b) are in **bold**.

4′,6-Diamidino-2-Phenylindole, Dihydrochloride (DAPI)					
Assignment (vibrational mode)	*Calculated (cm^{-1})*		*Experimental (cm^{-1})*		Comments
	Isolated DAPI molecule	DAPI hydrated by 5H_2O molecules	DAPI suspension/saturated solution in H_2O	Solid DAPI	
Asym. $\nu(OH_2)$	=	3857–3804	=	=	=
Sym. $\nu(OH_2)$	=	3756–3715	=	=	=
Pyrrolic ν(N-H)	3651	3488	3469	3463	=
Asym. terminal $\nu(N\text{-}H_2)$	3631	3567,3556			=
Sym. terminal $\nu(N\text{-}H_2)$	3525	3471,3437,3407	3330	3322	Coupled with ν(O-H)
Terminal ν(N-H)	3413,3415	3422,3421	3255	3255	=
Pyrrolic ν(C-H)	3249	3250	3186 (shoulder)	3199	=
Sym. vicinal ν(C-H)	3202–3199	3218,3201,3195	3108	3110	=
Asym. vicinal ν(C-H)	3185–3176	3184,3181,3172	3075	3080	=
?	=	=	2730	2729	1st δ(N-H) harmonic (calc. 1450)
Terminal ν(C-NH)	1710,1707	1716,1699 [coupled to $\delta(N\text{-}H_2)$]	1670 (with additional shoulder)	1667	=
$\delta(H_2O$ molecules)	=	1676–1644	1608	=	Probably shifted by H-bonds in the aqueous environment
Ring vibrations	1670,1661	1669, 1605	=	=	Mixed with δ(N-H)
$\delta(N\text{-}H_2)$	1618–1615	1642, 1620	1608	1609	=
Central ν(C-C)	1584	1580	1585	1585	=
In-plane pyrrolic δ(N-H), δ(C-H)	1540	1614 (coupled to ring vibrations at 1669,1605)	1608	1609	=
In-plane δ(C-H)	1528	1528	1559,**1544**(broad), 1522, **1506**	**1544**, 1524, **1503**	=
In-plane δ(N-H), $\delta(N\text{-}H_2)$, δ(C-H) + pyrrolic ν(C-NH)	1453	1548,1488,1468			
In-plane δ(N-H)	1425,1420	1450 [coupled to ν(C-NH2)], 1439	**1483**,**1463**	**1480**,**1460**	=
Ring vibrations	1403,1397 1349,1341	1413 1399,1349	**1433**,**1378**	**1433**,**1376**	=
Pyrrolic δ(N-H)	1254	1358 (coupled to several other modes)	**1329** (broad)	**1328**	=
δ(C-H), terminal δ(N-H)	1210, 1176, 1152,1147	1227, 1238,1281	1269, 1252, 1213,1205	1268, 1249, 1214, 1204	=
$(N\text{-}H_2)$ rock [coupled with δ(N-H), δ(C-H)]	1132, 1129, 1121	1190	1171 (weak)	1171	Intensity does not match
In-plane δ(N-H), $\delta(N\text{-}H_2)$	=	1186			
In-plane δ(C-H)	=	1144	1128? (weak)	1130	=
$\nu(C\text{-}NH_2)$	1090,1084	1169, 1072	1087,1064	1087, 1076, 1065	Coupled with CH bends
Out-of-plane δ(C-H), δ(N-H)	1003–812	973–775	867–773	867–776	=

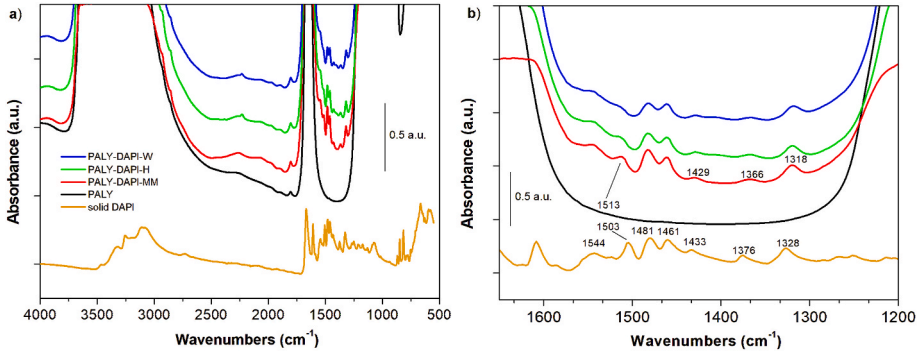

Fig. 6. FT-IR spectra of PALY, solid DAPI and the '*PALY@DAPI*' composite in all synthesis steps. a) full range; b) magnification of the fingerprint region. Spectra have been shifted on the Y-axis for sake of clarity.

These bands, associated with ring vibrations, are rather insensitive to the molecular environment. Besides, other DAPI modes show more or less marked differences (Fig. 6b), such as:

i) a band at 1544 cm^{-1} in solid DAPI (N-H, $N\text{-}H_2$ bending and C-H bending + pyrrolic C–N-H stretching: Table 2) shows no change, but a close one at 1503 cm^{-1} (1506 cm^{-1}, for DAPI suspended in H_2O: Table 2) with the same attributions blue-shifts in the composite at 1513 cm^{-1}, reducing its intensity. This suggests that the amino groups of DAPI (terminal and pyrrolic) might have a predominant bending character, being involved in H-bonding interactions which become stronger when adsorbed on PALY;
ii) two weak bands at 1433 and 1376 cm^{-1} in solid DAPI (ring vibrations; Table 2) shift at lower frequencies in the adduct, reaching 1429 and 1366 cm^{-1}. This indicates that, when adsorbed on PALY, the central part of the DAPI molecule (including the rings) may 'sense' a different surrounding (i.e., isolated rather

than stacked with one another, such as in the crystal), suggesting that monomers of the dye could interact with the host;

iii) a strong band at 1328 cm^{-1} in solid DAPI (1329 cm^{-1} in aqueous suspension; Table 2), assigned to pyrrolic N-H bending, red-shifts in the composite at 1318 cm^{-1}, further suggesting that the central region of the molecule might face different surroundings – i.e., in terms of H-bonding interactions – while interacting with PALY.

In **PALY + DAPI H**, no spectral change is observed but a slight intensity decay of the 1513 cm^{-1} band, further stressed in **PALY + DAPI W** (Fig. 6b). These outcomes confirm that specific interactions *do* form between PALY and DAPI *already* after grinding and provide hints about their nature – i.e., H-bonds between the amine groups of DAPI and the water molecules on the PALY laths surface. Heating and washing in H_2O have negligible effects in strengthening these bonds – and might even be responsible for their weakening.

3.6. Thermogravimetric analysis

TGA in N_2 and dried air were performed on PALY and on the '*PALY@DAPI*' adduct in all synthesis steps, with quite similar trends (Fig. 7 for curves in N_2; Supporting Information, Fig. S13, for those in dried air). In order to discriminate the first dehydration step at lower temperature, which for such a hygroscopic material depends spuriously on the starting environmental conditions, the TGA curves were aptly scaled to yield 100 % weight at 130 °C. TGA curves of DAPI in N_2 and dried air were also collected (insets in Fig. 7 and Fig. S9), showing a sharp decomposition step at ≈ 355 °C. The TGA of PALY, consistently with literature [20,32], has three distinct weight losses in the 25–500 °C range, roughly related to the release of the various kinds of water (physisorbed, zeolitic H_2O and structural OH_2).

The curves collected on the '*PALY@DAPI*' adduct in all synthesis steps follow a trend similar to that of PALY – though the global weight loss of the pure clay is lower. In detail, such a weight loss is slightly higher for **PALY + DAPI MM**, intermediate for **PALY + DAPI H** and lesser for **PALY + DAPI W**. This behavior is consistent with a progressive loss of the guest organic content while heating and washing. However, a direct estimation of the dye amount effectively adsorbed on the host is troublesome, as these data are inevitably biased by the different starting hydration levels of the samples. Such an effect, in fact, is mitigated – but not completely eliminated – by the applied scaling of the curves. Though following a similar trend, the global weight losses in air (Supporting Information, Fig. S9) are slightly higher, consistently with a more complete oxidation of the dye.

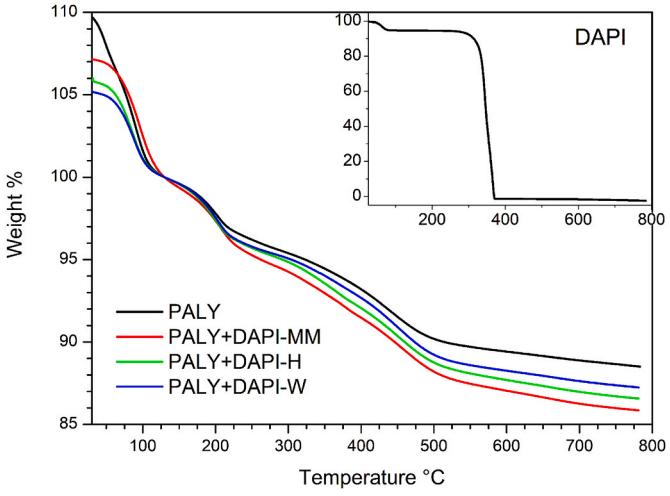

Fig. 7. Thermogravimetric curves in N_2 in the 25–800 °C range of PALY (black) and the '*PALY@DAPI*' adduct in all synthesis steps: **PALY + DAPI-MM** (red), **PALY + DAPI H** (green), **PALY + DAPI W** (blue). In the inset, the TGA curve of solid DAPI is reported.

A comparison of the derivative curves – in both N_2 and dried air (Supporting Information, Figs. S14 and S15, for those in dried air) – shows that a feeble derivative peak exists at ≈ 370 °C in the '*PALY@DAPI*' adduct, which does not occur in pure PALY. This peak is observed, albeit with a progressively reduced intensity, in all synthesis steps. The related weight loss (quantifiable in less than 1 wt %) might indeed account for the thermal degradation of the DAPI fraction conjugated to the host. As such an event peaks at ≈ 355 °C for the pure dye, we should conclude that complexation with PALY should enhance, albeit slightly, the thermal stability of DAPI. Its recurrence in all steps confirm that the interactions responsible for stabilizing the dye onto the host do form *already* after grinding.

4. Discussion

A quite stable '*Mayan*-inspired' fluorophore can be obtained by grinding PALY with 2 wt % of DAPI, following (at least partly) the recipe used for *Maya Blue*. However, some steps essential for *Maya Blue* preparation – i.e., heating at T ≥ 120 °C [20,69,70] – are ineffective here, causing instead a decay of the adduct. DAPI forms a stable complex if ground to PALY, but its steadiness is neither improved nor strengthened by heating or washing.

After grinding, the PALY laths tend to group in pairs or triplets – their adhesion possibly also being favoured by the efficient dispersion of DAPI monomers on the {100}, {110} and {010} faces. A significant decrease in the exposed BET-SSA is recorded too. Grinding is important for producing these PALY-based composites [36,37,93]. It favours detangling of the fibres, shortening their length and favouring cleavage mostly on the (110) crystal planes (Figs. 1 and 8), due to breaking of some Si-O-Si bonds (i.e., where the bridging oxygen links two SiO_4^{4-} tetrahedrons with oppositely oriented apical oxygens). As such, it is responsible for the 'edge' or 'surface-damage' effect, which causes exposure of Si-O^- groups on the cleavage surfaces [94,95]. Though most of them rapidly turn to silanols, this causes PALY to acquire temporarily a diffused negatively charged surface, which favours sorption of positively charged ions and molecules – a process possibly enhanced by temperature rise [31,37,96–98].

In composite materials, the surface charge of the hosting matrix affects the sorption capacity of (even partially) charged guests. Cationic $DAPI^{2+}$ (Fig. 1d) [87] is attracted by PALY – an interaction possibly involving the dye acetamidine fragments (similarly to what occurs for other supramolecular systems) [49] and the Si–O^- groups on the clay surface. Its molecule (17.4 Å × 6.3 Å, almost planar) [83] could be accommodated in the surface grooves that carve the {100}, {110} and {010} faces of the PALY laths, or even stuck at the edges of the tunnels on the {001} face (Figs. 1 and 8). Full encapsulation of the dye in the clay tunnels (supposed for other PALY-based adducts) [29,30,32,33] seems unlikely, due to molecular impediment and to the lack of a driving force favouring deep penetration. In *Maya Blue*, this force is represented by the heat-driven desorption of zeolitic H_2O and substitution with indigo. Since the stability of '*PALY@DAPI*' does not improve upon heating, this should be ruled out here. A surface interaction is also consistent with the micropore volume measures and justifies the enhancement in the QY of DAPI when ground to PALY (Table 1).

This electrostatic interaction is also supported by the red-shift of the main '*PALY@DAPI*' UV–Vis band after grinding with respect to DAPI in aqueous solution, implying a ground-state stabilization of a positively charged guest on a negative host [78]. This is confirmed by the high affinity of DAPI for other negatively charged matrices (e.g., DNA, SDS micelles and bis(2-ethylhexyl) sulfosuccinate (AOT)/isooctane reverse micelles). Similar interactions occur when DAPI binds to bovine serum albumin (BSA) [99] and DNA phosphate backbone, with a slight fluorescence increase [100,101]. Also, encapsulation of $DAPI^{2+}$ in self-assembling supramolecular systems based on Pillar [5]

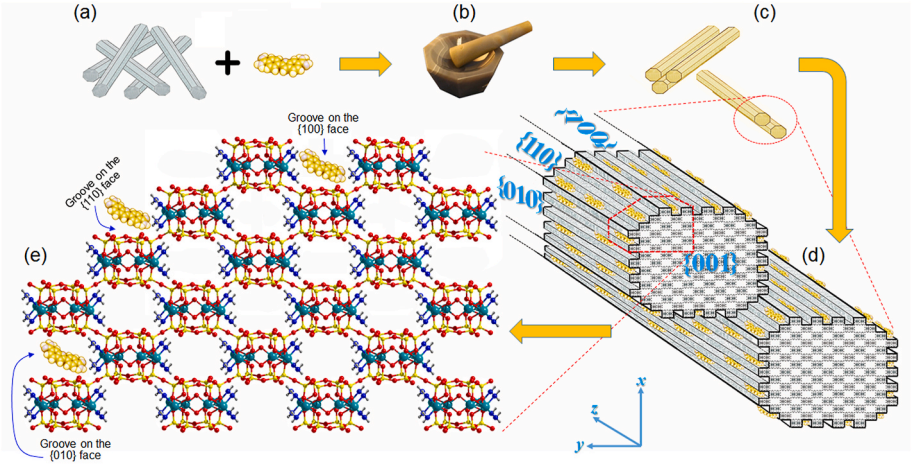

Fig. 8. Schematic recap of the efficient synthesis of the '*PALY@DAPI*' hybrid composite: (a) by mixing and grinding purified PALY and DAPI in an agate mortar (b), a yellowish adduct is formed in which the PALY fibrils (laths) tend to group in parallel oriented couples and/or triplets (c). By increasing magnification (c), the homogeneous distribution of the DAPI monomers on the surface of the PALY laths becomes evident. When inspecting the crystal structure (d), the DAPI molecules are likely to be hosted within in the grooves carving the surface of the {110}, {100} and {010} faces of the PALY laths (mutual dimensions of the fibrils and crystal structure not in scale; zeolitic H_2O not shown for sake of clarity).

arenes-surfactants-interpolyelectrolyte complexes (IPECs) or sulfonate groups of sulfobutylether β-cyclodextrin (SBE_7b-CD) (with important pharmaceuticals and biomedical applications [49,88]) involves similar bonds. On the other hand, DAPI is *not* prone to interact with positively charged hydrophobic moieties (e.g., cetyltrimethylammonium bromide – CTAB – micelles), proving that charge interactions overwhelm hydrophobic ones when binding to matrices [78,88]. Besides, these red-shifts are not observed if the interactions are *not* electrostatic (e.g., in ssDNA@DAPI/LDH composite thin films, where the "co-assembly method" rules) [89,102,103].

In '*PALY@DAPI*', the electrostatic interactions form *before* heating, being triggered by grinding alone. Stabilization of DAPI in PALY also amplifies the composite QY, similarly to what occurs when this dye interacts with other layered substrates (e.g., ordered phospholipids structures) [87]. However, a two-step binding process responsible for formation of host/guest interactions (hinted for other DAPI-based complexes: e.g., with DNA AT clusters and phospholipid vesicles) [85,87] cannot be ruled out. Such an electrostatic affinity, in fact, may favour only initial attraction, since the negative charge of PALY due to the 'edge-damage' effect is only temporary. Long-lasting interaction might be stabilized by other bonds. FTIR suggests that H-bonds form between the DAPI N-H/N-H_2 groups (pyrrolic and terminal) and the PALY water molecules. Zeolitic H_2O and/or structural OH_2 are the most fitting candidates: the former still occupies the PALY structure after grinding; the latter is exposed in the grooves on the {110} faces, resulting from cleavage. This evolution may even favour the apt accommodation of DAPI within the PALY grooves (Fig. 8), justifying the raise in the composite QY.

Heating and washing have no positive effect on these interactions. A decay in the composite aspect becomes evident (PALY fibres are shorter and form messy aggregates) after these treatments. Fragmentation and detachment of guest molecules from the host matrix occurs, as hinted by several factors (i.e., the decrease in intensity of the TGA derivative peak at ≈ 370 °C, the reduced detection of Cl by EDS and the increase in the BET-SSA in all sequential synthesis steps). Heating causes an almost complete loss of zeolitic H_2O, undermining the stability of some of the previously formed host/guest interactions. This might also explain the intensity decay of the IR maxima and the collapse in the composite QY (Table 1).

5. Conclusions

A stable, easy-to-assemble, polyfunctional hybrid material with enhanced fluorescence can be prepared based on the assembly of PALY (a natural clay mineral) with DAPI (a relatively unstable fluorescent dye). The stability and fluorescence of this '*PALY@DAPI*' composite are compatible with a molecular recognition process, involving at first an electrostatic attraction between oppositely charged guest and host surface, followed by formation of H-bonds within the grooves that carve the surface of the PALY laths, ensuring an enduring dye stabilization.

This hybrid composite bears some practical interest for the synthesis of tailored metal-free fluorescent materials for spectrum manipulation technologies, sensors, and optical devices. In light of the fibrous morphology of the PALY laths, with inner structural tunnels and surface grooves along the fiber axis (Fig. 1), a further application could be the fabrication of oriented fluorophores. This adduct may also open up interesting chances in the field of imaging and design-targeted drug-delivery systems - e.g., behaving as a fluorescence biosensor for specific DNA sequences (due to the low toxicity of PALY for humans) [104,105] or as a fluorescent carrier for active substances [106]. As far as drug-delivery applications are concerned, an optimized controlled uptake/release of the dye through supramolecular association should also be taken into account. Encouraging perspectives are provided by recent studies, showing how some DAPI-based composites react to chemical stimuli (addition of metals or biomolecules: e.g., adamantylamine) ensuring dissociation of the complex and free dye regeneration [88].

CRediT authorship contribution statement

Roberto Giustetto: Writing – original draft, Validation, Methodology, Formal analysis, Data curation, Conceptualization. **Gabriele Ricchiardi:** Methodology, Formal analysis, Data curation, Conceptualization. **Francesca Bonino:** Methodology, Formal analysis, Data curation. **Nadia Barbero:** Methodology, Formal analysis, Data curation.

Declaration of competing interest

The authors declare that they have no known competing financial interests or personal relationships that could have appeared to influence the work reported in this paper.

Data availability

Data will be made available on request.

Acknowledgements

The authors wish to thank Maria Carmen Valsania and Valentina Crocellà for their invaluable contributions in collecting FE-SEM data and N_2 adsorption/desorption measurements, respectively. GR, FB and NB acknowledge support from the Project CH4.0 under the MUR program "Dipartimenti di Eccellenza 2023–2027" (CUP: D13C22003520001).

Appendix A. Supplementary data

Supplementary data to this article can be found online at https://doi.org/10.1016/j.micromeso.2024.113196.

References

[1] G. D'Avino, L. Muccioli, F. Castet, C. Poelking, D. Andrienko, Z.G. Soos, et al., J. Phys. Condens. Matter 28 (2016) 433002, https://doi.org/10.1088/0953-8984/28/43/433002.
[2] U.W. Pohl, Electronic properties of organic semiconductors, in: U.W. Pohl (Ed.), Epitaxy of Semiconductors: Physics and Fabrication of Heterostructures, Springer International Publishing, Cham, Switzerland, 2020, pp. 177–205, https://doi.org/10.1007/978-3-030-43869-2_5. Graduate Texts in Physics.
[3] S. Kera, H. Yamane, N. Ueno, Prog. Surf. Sci. 84 (2009) 135–154, https://doi.org/10.1016/j.progsurf.2009.03.002.
[4] A. Mailman, A.A. Leitch, W. Yong, E. Steven, S.M. Winter, R.C.M. Claridge, et al., J. Am. Chem. Soc. 139 (2017) 2180–2183, https://doi.org/10.1021/jacs.6b12814.
[5] R. Haldar, M. Kozlowska, M. Ganschow, S. Ghosh, M. Jakoby, H. Chen, et al., Chem. Sci. 12 (2021) 4477–4483, https://doi.org/10.1039/D0SC07073D.
[6] R. Schlesinger, Y. Xu, O.T. Hofmann, S. Winkler, J. Frisch, J. Niederhausen, A. Vollmer, S. Blumstengel, F. Henneberger, P. Rinke, M. Scheffler, N. Koch, Phys. Rev. B 87 (2013) 155311.
[7] A. Stanculescu, F. Stanculescu, Organic semiconductors for non-linear optical applications, in: S.L. Pyshkin, J. Ballato (Eds.), Optpelectronics - Materials and Devices', Intechopen, 2015, p. 496, https://doi.org/10.5772/59334. ISBN 978-953-51-2174-9.
[8] M. Kratzer, A. Matkovic, C. Teichert, J. Phys. D Appl. Phys. 52 (23) (2019) 383001.
[9] M. Mostaghimi, C.R.C. Rêgo, R. Haldar, C. Wöll, W. Wenzel, M. Kozlowska, Frontiers in Materials 9 (2022) 840644, https://doi.org/10.3389/fmats.2022.840644.
[10] E. Conterosito, I. Benesperi, V. Toson, D. Saccone, N. Barbero, L. Palin, C. Barolo, V. Gianotti, M. Milanesio, ChemSusChem 9 (11) (2016) 1279–1289.
[11] A. Doménech, F.M. Valle-Algarra, M.T. Doménech-Carbò, M.E. Domine, L. Osete-Cortina, J.V. Gimeno-Adelantado, Appl. Mater. Interfaces 5 (2013) 8134–8145.
[12] M. Suárez, E. García-Romero, Clay Clay Miner. 61 (2013) 461–472.
[13] J.E. Chisholm, Can. Mineral. 28 (1990) 329–339.
[14] J.E. Chisholm, Can. Mineral. 30 (1992) 61–73.
[15] E. García-Romero, M. Suárez, Am. Mineral. 99 (2014) 1653–1661.
[16] G. Ferraris, E. Makovicky, S. Merlino, Crystallography of Modular Materials, IUCr. Oxford University Press, Oxford, 2008.
[17] R. Giustetto, G. Chiari, Eur. J. Mineral 16 (2004) 521–532.
[18] J.E. Post, P.J. Heaney, Am. Mineral. 93 (2008) 667–675.
[19] G. Chiari, R. Giustetto, J. Druzik, E. Dohene, G. Ricchiardi, Appl. Phys. A 90 (2008) 3–7.
[20] R. Giustetto, F. Llabrés i Xamena, G. Ricchiardi, S. Bordiga, A. Damin, R. Gobetto, M.R. Chierotti, J. Phys. Chem. B 109 (2005) 19360–19368.
[21] R. Giustetto, D. Levy, G. Chiari, Eur. J. Mineral 18 (2006) 629–640.
[22] M. Sánchez del Río, A. Doménech, M.T. Doménech-Carbó, M.L. Vázquez de Agredos Pascual, M. Suárez, E. García-Romero, The Maya blue pigment, in: E. Galàn, A. Singer (Eds.), Developments in Palygorskite-Sepiolite Research, A New Outlook on These Nanomaterials, Elsevier B.V., Amsterdam, 2011, pp. 453–481.
[23] A. Doménech, M.T. Doménech-Carbò, M. Sánchez Del Rìo, M.L. Vàzquez de Agredos Pascual, J. Solid State Electrochem. 13 (2009) 869–878.
[24] F. Ovarlez, S. Giulieri, A.M. Chaze, F. Delamare, J. Raya, J. Hirschinger, Chem. Eur J. 15 (2009) 11326–11332.
[25] S. Li, B. Mu, X. Wang, A. Wang, Dyes Pigments 190 (2021) 109322–109332.
[26] D. Reinen, P. Köhl, C. Muller, Z. Anorg. Allg. Chem. 630 (2004) 97–103.
[27] L.A. Polette-Niewold, F.S. Manciu, B. Torres, M. Alvarado Jr., R.R. Chianelli, J. Inorg. Biochem. 101 (2007) 1958–1973.
[28] F.S. Manciu, A. Ramirez Caro, W. Durrer, J. Govani, R.R. Chianelli, J. Raman Spectrosc. 39 (2008) 1257–1261.
[29] R. Rondão, J.S. Seixas de Melo, J. Phys. Chem. C 117 (1) (2013) 603–614.
[30] Z. Wei, L. Hong, X. Tingting, J. Yeling, D. Shijie, C. Jing, RSC Adv. 4 (2014) 51978–51983.
[31] R. Giustetto, O. Wahyudi, Microporous Mesoporous Mater. 142 (2011) 221–235.
[32] R. Giustetto, K. Seenivasan, D. Pellerej, G. Ricchiardi, S. Bordiga, Microporous Mesoporous Mater. 155 (2012) 167–176.
[33] R. Giustetto, J.G. Vitillo, I. Corazzari, F. Turci, J. Phys. Chem. B 118 (2014) 19322–19337.
[34] R. Giustetto, A. Idone, E. Diana, J. Raman Spectrosc. 48 (4) (2017) 507–517.
[35] R. Giustetto, Acta Phys. Pol., A 135 (5) (2019) 1123–1125.
[36] H. Chen, J. Zhao, A. Zhong, Y. Jin, Chem. Eng. J. 174 (2011) 143–150.
[37] H. Chen, A. Zhong, J. Wu, J. Zhao, H. Yan, Ind. Eng. Chem. Res. 51 (2012) 14026–14036.
[38] B. Mu, A. Wang, J. Environ. Chem. Eng. 4 (2016) 1274–1294.
[39] G. Verri, C. Clementi, D. Comelli, S. Cather, F. Piqué, Appl. Spectrosc. 62 (12) (2008) 1295–1302.
[40] W. Li, G. Zheng, Photochem. Photobiol. Sci. Mar. 11 (3) (2012) 460–471.
[41] O. Tagit, N. Hildebrandt, ACS Sens. 2 (1) (2017) 31–45.
[42] Q. Wang, B. Mu, Y. Zhang, J. Zhang, A. Wang, Microporous Mesoporous Mater. 224 (2016) 107–115.
[43] C. Ouellet-Plamondon, P. Aranda, A. Favier, G. Habert, H. van Dammed, E. Ruiz-Hitzkyb, RSC Adv. 5 (2015) 98834–98841.
[44] G.T.M. Silva, K.M. da Silva, C.P. Silva, A.C.B. Rodrigues, J. Oake, M.H. Gehlen, C. Bohne, F.H. Quina, Photochem. Photobiol. Sci. 18 (2019) 1750–1760.
[45] M.H. Räz, M. Hollenstein, Mol. Biosyst. 11 (2015) 1454–1461.
[46] T. Nagata, S. Shinya, T. Ohnuma, T. Fukamizo, Nature Sci. Rep. 11 (2021) 2494, https://doi.org/10.1038/s41598-021-81903-3.
[47] B. Martin, P.D. Dans, M. Wieczór, N. Villegas, I. Brun-Heath, F. Battistini, M. Terrazas, M. Orozco, PLoS Comput. Biol. 18 (1) (2022) e1009749, https://doi.org/10.1371/journal.pcbi.1009749.
[48] J. Kapuscinski, Biotech. Histochem. 70 (5) (1995) 220–233, https://doi.org/10.3109/10520299509108199.
[49] A. Nazarova, A. Khannanov, A. Boldyrev, L. Yakimova, I. Stoikov, Int. J. Mol. Sci. 22 (2021) 6038–6056.
[50] T.A. Larsen, D.S. Goodsell, D. Cascio, K. Grzeskowiak, R.E.J. Dickerson, J. Biomol. Struct. Dyn. 7 (1989) 477–491.
[51] E. Trotta, M. Paci, Nucleic Acids Res. 26 (1998) 4706–4713.
[52] S.K. Kim, S. Eriksson, M. Kubista, B. Norden, J. Am. Chem. Soc. 115 (1993) 3441–3447.
[53] W.D. Wilson, F.A. Tanious, H.K. Barton, R.L. Jones, K. Fox, R.L. Wydra, L. Strekowski, Biochemistry 29 (1990) 8452–8461.
[54] E. Trotta, E. D'Ambrosio, G. Ravagnan, M. Paci, Nucleic Acids Res. 23 (1995) 1333–1340.
[55] E. Trotta, E. D'Ambrosio, G. Ravagnan, M. Paci, J. Biol. Chem. 271 (44) (1996) 27608–27614.
[56] D. Vlieghe, J. Sponer, L.V. Meervelt, Biochemist 38 (1999) 16443–16451.
[57] P. Colson, C. Bailly, C. Houssier, Biophys. Chem. 58 (1996) 125–140.
[58] S. Eriksson, S.K. Kim, M. Kubista, B. Norden, Biochemistry 32 (1993) 2987–2998.
[59] F.J. Green, Sigma-Aldrich Handbook of Stains, Dyes and Indicators, 1990, p. 244.
[60] J. Kapuscinski, W. Szer, Nucleic Acids Res. 6 (1979) 3519.
[61] W.C. Russell, C. Newman, D.H. Williamson, Nature 253 (1975) 461–462.
[62] C.F. Brunk, K.C. Jones, T.W. James, Anal. Biochem. 92 (1979) 497–500.
[63] F.A. Tanious, J.M. Veal, H. Buczak, L.S. Ratmeyer, W.D. Wilson, Biochemistry 31 (1992) 3103–3112.
[64] J. Kapuscinski, J. Histochem. Cytochem. 38 (9) (2017) 1323–1329, https://doi.org/10.1177/38.9.1696951.
[65] R. Giustetto, D. Levy, O. Wahyudi, G. Ricchiardi, J.G. Vitillo, Eur. J. Mineral 23 (2011) 449–466.
[66] R. Giustetto, O. Wahyudi, I. Corazzari, F. Turci, Appl. Clay Sci. 52 (1–2) (2011) 41–50.
[67] R. Giustetto, R. Compagnoni, Clay Miner. 46 (2011) 371–385.
[68] W. Wang, A. Wang, Appl. Clay Sci. 119 (2016) 18–30.
[69] H. Van Olphen, Science 154 (1966) 645–646.
[70] R. Kleber, L. Masschelein-Kleiner, J. Thissen, Stud. Conserv. 12 (1967) 41–55.
[71] M. Sànchez Del Rìo, P. Martinetto, C. Reyes-Valerio, E. Dooryhée, M. Suárez, Archaeometry 48 (1) (2006) 115–130.
[72] Gaussian 16, Revision B.01, M. J. Frisch, G. W. Trucks, H. B. Schlegel, G. E. Scuseria, M. A. Robb, J. R. Cheeseman, G. Scalmani, V. Barone, G. A. Petersson, H. Nakatsuji, X. Li, M. Caricato, A. V. Marenich, J. Bloino, B. G. Janesko, R. Gomperts, B. Mennucci, H. P. Hratchian, J. V. Ortiz, A. F. Izmaylov, J. L. Sonnenberg, D., Williams-Young, F. Ding, F. Lipparini, F. Egidi, J. Goings, B. Peng, A. Petrone, T. Henderson, D. Ranasinghe, V. G. Zakrzewski, J. Gao, N. Rega, G. Zheng, W. Liang, M. Hada, M. Ehara, K. Toyota, R. Fukuda, J. Hasegawa, M. Ishida, T. Nakajima, Y. Honda, O. Kitao, H. Nakai, T. Vreven, K. Throssell, J. A. Montgomery, Jr., J. E. Peralta, F. Ogliaro, M. J. Bearpark, J. J. Heyd, E. N. Brothers, K. N. Kudin, V. N. Staroverov, T. A. Keith, R. Kobayashi, J. Normand, K. Raghavachari, A. P. Rendell, J. C. Burant, S. S. Iyengar, J. Tomasi, M. Cossi, J. M. Millam, M. Klene, C. Adamo, R. Cammi, J. W. Ochterski, R. L. Martin, K. Morokuma, O. Farkas, J. B. Foresman, and D. J. Fox, Gaussian, Inc., Wallingford CT (2016)..
[73] S. Caillère, S. Henin, in: G. Brown (Ed.), X-Ray Identification and Crystal Structure of Clay Minerals, Mineralogical Society, London, 1961, pp. 343–353.
[74] M.C. Leaper, M.S.A. Bradley, J.A.S. Cleaver, I. Bridle, A.R. Reed, H. Abou-Chakra, U. Tüzün, Adv. Powder Technol. 13 (4) (2002) 411–424.
[75] A. Fukunishi, Y. Mori, Adv. Powder Technol. 17 (5) (2006) 567–580.
[76] A. Doménech, M.T. Doménech-Carbò, M.L. Vàzquez de Agredos Pascual, J. Phys. Chem. B 110 (2006) 6027–6039.
[77] M. Suàrez, J. García-Rivas, J. Morales, A. Lorenzo, A. García-Vicente, E. García-Romero, Appl. Clay Sci. 216 (2022) 106311–106322.

[78] D. Banerjee, S.K. Pal, J. Phys. Chem. A 112 (2008) 7314–7320.
[79] R. Prajapati, S. Chatterjee, K.K. Kannaujiyab, T.K. Mukherjee, Nanoscale 8 (2016) 13006–13016.
[80] J. Durmis, M. Karvaš, Z. Mañásek, Collect. Czech Chem. Commun. 38 (1973) 224–242.
[81] M. Kubista, B. Ákerman, B. Albinsson, J. Am. Chem. Soc. 111 (1989) 7031–7035.
[82] E.M. Digby, R. Rana, M. Nitzb, A.A. Beharry, Chem. Comm. 55 (2019) 9971–9974.
[83] G. Manzini, M.L. Barcellona, M. Avitabile, F. Quadrifoglio, Nucleic Acids Res. 11 (1983) 8861–8876.
[84] M. Kubista, B. Ákerman, B. Nordén, Biochemistry 26 (1987) 4545–4553.
[85] M.L. Barcellona, E. Gratton, Eur. J. Biophys. 17 (1990) 315–323.
[86] M.L. Barcellona, E. Gratton, Biochemistry 35 (1996) 321–333.
[87] R. Favilla, G. Stecconi, P. Cavatorta, G. Sartor, A. Mazzini, Biophys. Chem. 46 (1993) 217–226.
[88] Y. Hu, P. Zhang, R. Ma, X. Zhang, J. Lu, Biosens. Bioelectron. (2018), https://doi.org/10.29011/2577-2260.100038. Open Acc: BBOA-138.
[89] M.N. Shinde, A.C. Bhasikuttan, J. Mohanty, ChemPhysChem 16 (2015) 3425–3432.
[90] Y. Zhang, D.J.S. Birch, Y. Chen, Appl. Phys. Lett. 99 (2011) 103701–103703.
[91] M.L. Barcellona, E. Gratton, Biophys. Chem. 40 (1991) 223–229.
[92] M. Taniguchi, J.S. Lindsey, Photochem. Photobiol. 94 (2018) 290–327.
[93] H. Chen, J. Zhao, Adsorption 15 (2009) 381–389.
[94] S. Yariv, I. Lapides, J. Mater. Synth. Process. 8 (2000) 223–233.
[95] H. Chen, Y. Jin, A. Zhong, J. Wu, H. Yan, R. Li, J. Porous Mater. 29 (2022) 215–227, https://doi.org/10.1007/s10934-021-01158-1.
[96] H.H. Murray, Appl. Clay Sci. 17 (2000) 207.
[97] W. Kuang, G.A. Facey, C. Detellier, Clay Clay Miner. 52 (2004) 635–642.
[98] L. Wu, X. Liu, G. Lv, R. Zhu, L. Tian, M. Liu, Y. Li, W. Rao, T. Liu, L. Liao, Sci. Rep. 11 (2021) 10640, https://doi.org/10.1038/s41598-021-90235-1.
[99] A. Mazzini, P. Cavatorta, M. Iori, R. Favilla, G. Sartor, Biophys. Chem. 42 (1992) 101–109.
[100] G. Manzini, L. Xodo, M.L. Barcellona, F. Quadrifoglio, J. Biosci. 8 (3–4) (1985) 699–711.
[101] R. Huschka, O. Neumann, A. Barhoumi, N.J. Halas, Nano Lett. 10 (10) (2010) 4117–4122, https://doi.org/10.1021/nl102293b.
[102] Y. Qin, J. Shi, X. Gong, Z. Tian, P. Zhang, J. Lu, Adv. Funct. Mater. 26 (2016) 6752–6759.
[103] P. Zhang, Y. Hu, R. Ma, L. Li, J. Lu, J. Mater. Chem. B 5 (2017) 160–166.
[104] C. Viseras, A. Lopez-Galindo, Appl. Clay Sci. 14 (1–3) (1999) 69–82.
[105] M.L. de Gois da Silva, A. Campos Fortes, A. da Rocha Tomé, E.C. da Silva Filho, R. M. de Freitas, J.L. Soares-Sobrinho, C.M. da Silva Leite, M. Felts de La Roca Soares, Brazilian Journal of Pharmaceutical Sciences 49 (4) (2013) 729–736.
[106] M. De Santo, A. Giovinazzo, M. Fava, E. Mazzotta, I.E. De Napoli, M. Greco, A. Comandé, A. Nigro, P. Argurio, I. Perrotta, M. Davoli, A. Tagarelli, R. Elliani, T. Granato, G. Nicolini, A. Chiorazzi, S. Semperboni, E. Ballarini, C. Crocamo, G. Cavaletti, D. Lombardo, D. Sisci, C. Morelli, A. Leggio, L. Pasqua, Mater. Chem. Front. 7 (2023) 216–229.